Structural Engineering and Mechanics, *Vol. 78, No. 4 (2021) 455-471*
DOI: https://doi.org/10.12989/sem.2021.78.4.455

Structural behavior of concrete walls reinforced with ferrocement laminates

Yousry B.I. Shaheen[1a], Hala M. Refat[2b] and Ashraf M. Mahmoud*[3]

[1]*Civil Engineering Department, Faculty of Engineering, Menoufia University, Menoufia, Egypt*
[2]*Civil Engineering Department, Faculty of Engineering, Benha University, Benha, Egypt*
[3]*Civil Engineering Department, Faculty of Engineering, Modern University for Technology and Information (MTI), Al-Mokattam, Cairo, Egypt*

(*Received November 5, 2019, Revised March 25, 2021, Accepted April 6, 2021*)

Abstract. The present work focuses on experimental and numerical performance of the ferrocement RC walls reinforced with welded steel mesh, expanded steel mesh, fiber glass mesh and tensar mesh individually. The experimental program comprised twelve RC walls having the dimensions of 450 mm×100 mm×1000 mm under concentric compression loadings. The studied variables are the type of reinforcing materials, the number of mesh layers and volume fraction of reinforcement. The main aim is to assess the influence of engaging the new inventive materials in reinforcing the composite RC walls. Non-linear finite element analysis; (NLFEA) was carried out to simulate the behavior of the composite walls employing ANSYS-10.0 Software. Parametric study is also demonstrated to check out the variables that can mainly influence the mechanical behavior of the model such as the change of wall dimensions. The obtained numerical results indicated the acceptable accuracy of FE simulations in the estimation of experimental values. In addition, the strength gained of specimens reinforced with welded steel mesh was higher by amount 40% compared with those reinforced with expanded steel mesh. Ferrocement specimens tested under axial compression loadings exhibit superior ultimate loads and energy absorbing capacity compared to the conventional reinforced concrete one.

Keywords: ferrocement; RC walls; composite material; experimental; NLFE modeling; Ansys-10

1. Introduction

Ferrocement is a special type of reinforced concrete. Ferrocement primarily differs from conventional reinforced concrete and prestressed concrete by mainly in the manner by which reinforcing elements are dispersed and arranged. It consists of cement mortar matrix reinforced with closely spaced, multiple layers of mesh or fine rods completely impregnated with cement mortar. It has a wide variety of metallic reinforcing mesh materials; woven wire mesh, welded wire mesh and expanded metal mesh. Ferrocement is ideally appropriate for structures in which preponderant membrane stresses take place. Much work has been conducted on the ferrocement as a low cost construction material and a flexible structural system, and many parameters were investigated to validate the new system and to enhance its performance. As a result, ferrocement has been substantially used to assemble different element such as, tanks, roofs, bridge decks…etc. The RC wall is one of the most considerable and critical element that can appoint the behavior and failure mode of the structure. In the last few decades, incidence of failures of reinforced concrete structures has been seen widely because of increasing service or seismic loads problems.

Basunbul *et al*. (1990) studied the structural behavior of ferrocement sandwich load bearing wall panels. The effect of the amount of wire mesh reinforcement and the presence of skeletal steel was investigated accordance with ASTM E73-77. As a result, ferrocement wall panels reinforced with wire mesh only exhibited ductility than panels that contained the same amount of wire mesh in addition to skeletal steel. On the other hand, Al-Rifiaie and A-Aziz (1995) accomplished an investigation to study the behavior of ferrocement under axial compression loading for the load bearing precast wall panels with box type cross section. The proposed model exhibited more efficient the appearance of the initial cracks, load carrying capacity, ductility and energy absorption values. In (2004), Fahmy *et al*. and Gaafar conducted a research on the ferrocement panels for use as floor units. Ferrocement sandwich panels and hollow core panels were investigated as flexural slabs, employing light brick core and foam concrete. Shear connectors in the form of Z-shaped steel bars were used. The proposed model exhibited higher ultimate and serviceability loads, more crack resistance control, high ductility, and good energy absorption properties than the equivalent RC panels. In addition, Memon *et al.* (2004) discussed the results of an experimental investigation on sandwich blocks fabricated using lightweight aerated concrete encased in a ferrocement box. A significant increase in compressive strength due to the encasement of aerated concrete was illustrated. Furthermore, Fahmy *et al.* (2004) presented a research to develop ferrocement sandwich and hollow core panels for use as floor and wall bearing units. The proposed panels are

*Corresponding author, Associate Professor
E-mail: drmahmoud@eng.mti.edu.eg
[a]Professor
E-mail: Ybishaheen@yahoo.com
[b]Associate Professor
E-mail: hala.abusafa@bhit.bu.edu.eg

ISSN: 1225-4568 (Print), 1598-6217 (Online)

lighter in weight relative to the conventional reinforced concrete panels. High ultimate and serviceability loads, crack resistance control, high ductility, and good energy absorption properties were achieved by using the proposed panels. Moreover, Shaheen *et al.* (2013) investigated the impact resistance of reinforced ferrocement concrete plates reinforced with various types of reinforcing materials. Results of reinforced ferrocement plates emphasized that, increasing the number of the steel mesh layers in the ferrocement composites increases energy at first cracking, energy at up to failure, and energy absorption properties. An experimental and numerical investigation to study the structural behavior of ferrocement wall panels when subjected to axial load was executed by Grija *et al.* (2014). An enhancement in terms of load - deflection relation, crack pattern distribution, strain distribution and ultimate loads were observed. Lakshmikandhan *et al.* (2015) established experimentally and numerically, a novel ferrocement wall panel in order to be more appropriate for the light weight and affordable building construction. In view of this, the wall panel is proposed with ferrocement skin with appropriate ribs to achieve the structural adequacy and constructability. The panel is found to be more uniform and better quality, and more suitable for the light weight building construction. In addition, Amin *et al.* (2015) improved the more effective use of ferrocement plate as a construction material by observing the homogeneity, porosity/voids, initial rate of absorption (IRA) and water absorption behavior of double layer wire mesh (DLWM) reinforced ferrocement plate. The outcomes prove that the homogeneity of the DLWM ferrocement is almost in regular manner, although contains large voids / porosity but fewer amount. On the other hand, Bezbradica (2015) presented an experimental and numerical investigation of the stiffness properties of three reinforcement materials for concrete shell structures including ferrocement, glass-fibre textile and carbon-fibre textile. The results show that the carbon-reinforced beam has the highest stiffness comparing to other reinforcing materials. Deshpande and Shirsath (2016) accomplished experimentally the effect of using different numbers of Bamboo mesh layers and spacing variation on the flexural strength of ferrocement beams. As a result, and though the flexural load carrying capacity of Bamboo mesh layers is lesser than conventional ferrocement layers, it is acceptable and can be used for light weight structures as a wall panels. Additionally, the experimental and numerical estimation of the flexural behavior of ferrocement ribbed plates reinforced with composite material is carried out by Shaheen *et al.* (2016). In view of this, high strength, ductility ratio and energy absorption properties of the proposed ribbed ferrocement plates were observed compared to the conventional RC ribbed plates. Ramasamy and Subramani (2016) investigated the behavior of ferrocement encased lightweight aerated mortar wall elements of relatively large size particularly in compression with additional thermal conductivity tests. In addition, the optimum high workability and high performance mortar were established. In addition, the minimum flow value (flow table) of cement mortar capable to be poured during the casting of thin ferrocement encasement was discussed. In (2017), Lakshmikandhan *et al.* carried out an experimental and analytical investigation of a simple, lightweight and cost effective technology for replacing the existing wall systems with lightweight sandwich panel cast with a lightweight concrete inner core and ferrocement outer skins. This lightweight wall panel is tested for in-plane compression loading. The result confirms the suitability of lightweight concrete infilled panels for the load bearing and non-load bearing walls. The performance of ferrocement infill wall panels was carried out by Rashid *et al.* (2019). It focused on the mechanical properties, water absorption and durability of a series of specimens casting with single and double steel wire mesh layers. Flexural performance was carried out following sixty days in temperature cycle and in corrosion cell. The test results showed that the flexural strength performance of the ferrocement panels was reduced by an amount from 52% to 35% for single and double layer wire mesh samples respectively followed by corrosion environment. The flexural behavior of ferrocement beams with lightweight cores, which were made of autoclaved aerated lightweight brick, extruded foam, and lightweight concrete cores, and were reinforced with expanded metal, and welded wire mesh was investigated by Shaaban *et al.* (2018). As results, ferrocement beams of light weight cores may be promising as an alternative to conventional beams and may be viable alternatives especially for low cost residential buildings. A comparison of the performance of full-scale exterior beam-column space joints in the traditionally reinforced existing buildings with those cast according to ACI 318 and the behavior of such joints after retrofitting by ferrocement layers under cyclic displacement-controlled cyclic loading was executed by Shaaban Seoud (2018). The joints retrofitted by ferrocement layers showed higher ultimate capacity, higher ultimate displacement, as observed for the traditionally reinforced one.

The main intention of this study is to create elements acting as wall bearing elements using the unique properties of ferrocement concept. These developed elements can exchange the conventional reinforced concrete elements because of their economical and lighter in weight. In addition, the study aimed at decreasing the cost of production of the new elements by using cheap materials like light weight, durable reinforcing materials such as polypropylene fibers, polyethylene mesh, fiber glass mesh, tensar mesh, expanded steel mesh and galvanized steel meshes. Twelve RC walls with various volume fraction of steel reinforcement and different number of metallic and non metallic mesh reinforcement layers were constructed and tested under vertical load until failure. Furthermore, the current research aims to simulate the tested ferrocement walls by means of finite element ANSYS-10 program to check out their mechanical behavior up to failure.

2. Experimental program

Walls test specimens were grouped into twelve designations according to the type of reinforcing materials used. All designations having the dimensions of 450 mm×

Table 1 Details of the designation specimens.

Designation	No. of layers	Reinforcement details (Metallic or non metallic)	Volume fraction % (V_{rL})	Specific Surface Area,cm^{-1}
*W*1 (Control)	-------	6 Φ 10 mm+7 Φ 6 / m (stirrups)	1.5054	0.07240
*W*2	one	one layer expanded steel mesh	0.4665	0.09350
*W*3	one	one layer expanded steel mesh+6 Φ 10 mm	0.9240	0.24158
*W*4	two	two layers expanded mesh	0.9330	0.18660
*W*5	two	two layers expanded steel mesh+6 Φ 10 mm	1.9809	0.33470
*W*6	two	two layers welded steel mesh	0.3710	0.01855
*W*7	two	two layers welded steel mesh+6 Φ 10 mm	1.4189	0.06047
*W*8	four	four layers welded steel mesh	0.7420	0.03710
*W*9	four	Four layers welded steel mesh+6 Φ 10 mm	1.7899	0.07902
*W*10	one	one layer tensar mesh+6 Φ 10 mm+3 Φ 6 mm (stirrups)	1.7519	0.15656
*W*11	one	one layer fiber glass mesh+6 Φ10 mm+3 Φ 6 mm (stirrups)	1.4749	0.10115
*W*12	one	one layer polyethylene mesh+6 Φ10 mm+3 Φ 6 mm (stirrups)	2.6039	0.23630

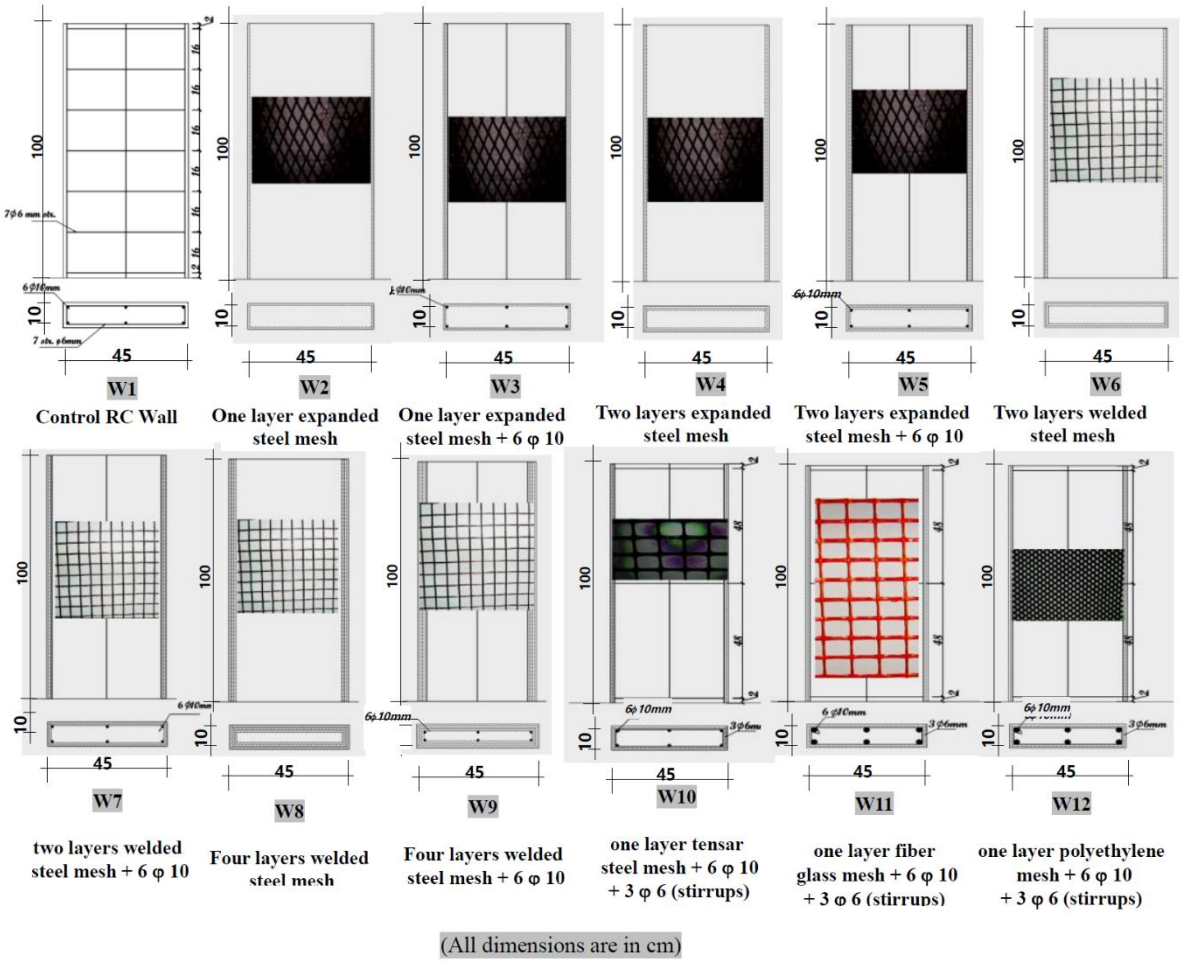

Fig. 1 Reinforcement arrangements for the designation walls

100 mm in cross section and 1000 mm long were reinforced with proposed composite materials. Table 1 presents the details of all selection specimens. Fig. 1 displays the reinforcement arrangements for all the twelve designations walls. Coarse aggregate was not utilized in the mortar to produce flow able mortar that can be cast easily into the molds without causing honeycombing. Super plasticizer was applied to contribute high workability to ease the process of casting. Different types of metallic and non metallic meshes were used. Several types of reinforcing materials were employed as demonstrated in Fig. 2. The longitudinal volume fraction is formalized according to the Ferrocement Model Code (2001) as follows

$$V_{rL} = \frac{Nn\pi d_w^{\ 2}}{4tB} \tag{1}$$

[For welded and woven wire mesh]

$$V_{rL} = .65\frac{NW_r}{t\gamma_r} \tag{2}$$

[For expanded wire mesh]

(a) Expanded steel mesh (b) Welded steel mesh (c) Tensar (d) Fiber glass mesh (e) Polyethelen

Fig. 2 Meshes used for reinforcement

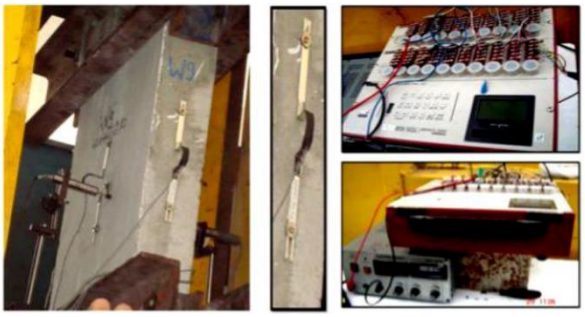

Fig. 3 Test setup and data logger used in recording results

Where:

B = width of the specimen

d_w = diameter of mesh wire

N = number of layers of mesh

n = number of bars in one layer in the cross section

t = thickness of ferrocement layer for calculating the volume fraction in the layer

= thickness of the web for calculating the volume fraction in the web

W_r = unit weight of reinforcing mesh

γ_r = density of reinforcing material

All produced test designations were tested under axial compression loadings until failure. The main constant parameters between all specimens were the wall dimension, and the main reinforced percentage for all walls, except walls *W*2, *W*4, *W*6, and *W*8, whose are reinforced by steel meshes only for comparison requirements. The main variables studied were the number of reinforcing mesh layers, type of mesh used, volume fraction of reinforcing steel and combination of mesh and skeletal steel bars. All test specimens were supplied with four displacement transducers (type P1) of gauge length 200 mm and was placed on four sides of the test specimen to measure the vertical displacement versus load during the test. In addition, two linear variable differential transducers (LVDT) were placed at the center of two opposite sides of the test specimen to measure the horizontal displacement.

All test specimens were tested under concentric loadings at the wall ends until failure. The main components of the testing facility are: Control Station, Loading Cells and Testing Frame. The load was applied via loading cell which was acting at the wall head. The load was incrementally applied with an increment of 5.0 to 20 kN for all the test specimens as shown in Fig. 3. All the deformation characteristics, cracking patterns and strengths were extensively measured at all stages of loadings.

2.1 Material properties

2.1.1 Cement

Ordinary Portland cement was used throughout this work (O.P.C) with a specific surface area (Blaine fineness) of 3050 cm^2/gm. Typical compounds of the cement was as follows: C_3S =65.1 percent, C_2S=7.6 percent, C_3A=10.8 percent and C_4AF=7.3 percent. The alkali content (as Na_2O equivalent) was 0.29 mass percent.

2.1.2 Silica fume

Silica fume (S.F.) was employed in the present work to enhance the strength of ferrocement mortar and/or concrete core. Based on Abdel Naby (2006), it was used as partial replacement 15% by weight of cement in the mortar mixtures. The S.F. had an average particle size of 0.1 micrometer and a silicon dioxide content of 93%.

2.1.3 Fine aggregates

Natural siliceous sand with a fineness modulus of 2.91, a saturated surface dry specific gravity of 2.51 and absorption of 0.50 percent was used in the present experimental work.

2.1.4 Chemical admixtures (Super plasticizer)

Super plasticizer complies with ASTM C494 type F, and B.S. 5075 part 3, with a specific weight of 1.2 at 20ºC was used to provide the necessary workability for concrete and mortar. The super plasticizer's commercial name is SIKAMINT 163M. The manufacturer recommended dosage is between 0.5-2 percent by weight of cementatious materials.

2.1.5 Synthetic fibers

Synthetic fibers were added to the mortar mix of the ferrocement laminate for all the tested specimens incorporating ferrocement forms. The added fibers, are commercially as "fiber mesh 300". According to the manufacturer published data, this type of fibers is 100 percent virgin homopolymer polypropylene fibrillated fibers containing no reprocessed olefin materials. This type of fibers is specifically engineered and manufactured in an ISO 9001:2000 certified facilities to an optimum gradation for use as concrete secondary reinforcement at a minimum of 0.1% by volume (0.9 kg/m^3). The fibers comply with National Building Codes and ASTM C III6/C III6M, Type III fiber reinforced concrete (2015).

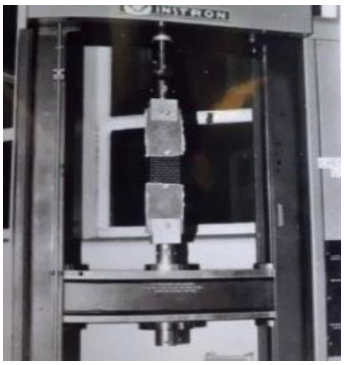

Fig. 4 Wire mesh

2.1.6 Reinforcing steel bars

High tensile deformed steel bars of diameter 10 mm were used to reinforce the control RC walls. Tensile tests were performed on three samples of the bars. The average test results of the three samples showed the proof stress and ultimate strength of the material were 551 MPa and 670 MPa respectively. Mild steel stirrups of diameter 6 mm were used as shear reinforcement for the control wall. The material has nominal yield stress of 240 MPa.

2.1.7 Expanded steel mesh

Expanded steel mesh of diamond size 32×14 mm, weight equal 1660 gm/m^2 and dimensions of wire 1.25×1.5 mm was used as reinforcing materials as shown in Fig. 2(a). Three samples of mesh were tested using the Universal Testing Machine as shown in Fig. 4 to investigate the mechanical properties. The mesh has a proof stress of 199 MPa, ultimate strength of 320 MPa, and modulus of elasticity 120 GPa.

2.1.8 Welded steel mesh

Welded square galvanized steel mesh of dimensions 12.5x12.5 mm and weight 600 gm/m^2 was employed as shown in Fig. 2(b). The mechanical properties were obtained experimentally as illustrated previously in Fig. 4. The mesh has a proof stress of 737 MPa, ultimate strength of 834 MPa and modulus of elasticity 170 GPa.

2.1.9 Polyethylene mesh

This type of mesh is made from high density polyethylene. "Geogrid CE 121" was used for this type of mesh as shown in Fig. 2(f). The mesh has opening size of 6x8 mm, thickness of 3.3 mm, and weight of 725 gm/m^2 and volume fraction of 2.04%. Tensile test was performed on the mesh and the results showed that this type of polyethylene mesh has strength of 24.7 MPa and extension of 21%.

2.1.10 Fiber glass mesh

Gavazzi "V3-133-A" was used for this type of mesh. Mesh has opening dimension of 12.5×11.5 mm. The cross section dimension of the fiber strings in the longitudinal direction is 1.66×0.66 mm and in the transverse direction is 1.0×0.5 mm as shown in Fig. 2(d). The mesh has weight of 123 gm/m^2 and volume fraction of 0.535%. The tensile test on this type of mesh showed that it has tensile strength in the longitudinal direction of 325 MPa and extension of 5.5%.

Table 2 Compressive strength of the concrete mortar

Designation	Average Ferrocement Mortar Compressive Strength (MPa)
*W*1, *W*2, *W*3, *W*4	40
*W*5, *W*6, *W*7, *W*8	39
*W*9, *W*10, *W*11, *W*12	38

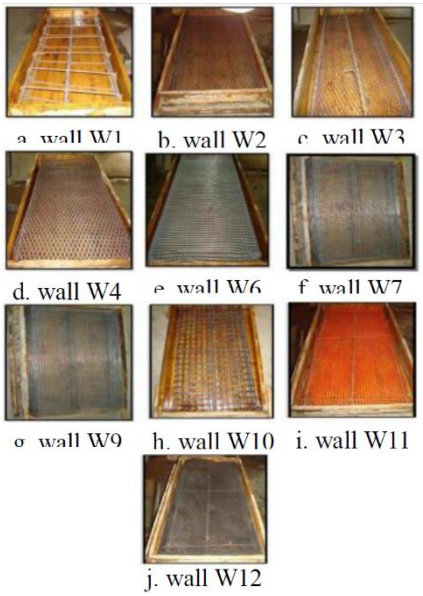

Fig. 5 Details of reinforcing materials of RC walls ready for casting

2.1.11 Tensar steel mesh

Tensar steel mesh with opening dimension of 6×8 mm, and weight 725 gm/m^2 was used as indicated in Fig. 2(c). The sheet used has a thickness of 3.30 mm. The proof stress of the mesh was 260 Mpa, and the modulus of elasticity was 100 Gpa.

2.2 Mix design

The materials used for the mix design were ordinary Portland cement, sand, silica fume and a super plasticizing agent. The main objectives of mix design was to determine the high amount of cement could be partially replaced by silica fume to increase strength of mortar matrix with no detrimental effects on the quality and properties of the mix in both the fresh and hardened states. The requirement of good workability was essential, to allow the mortar matrix to penetrate through the layers of steel mesh reinforcement. A super plasticizing agent was used to increase flow characteristics and accelerate the early strength development. Mortar mixtures for the ferrocement were made using a water to cement ratio of 0.4, sand to cement ratio of 2:1 and super-plasticizer of 2% by weight of cement, while 10% by weight of cement was replaced by S.F. The density of the mortar mix was approximately 2200 kg/m^3. The average compressive strength after 28 days was 35 MPa.

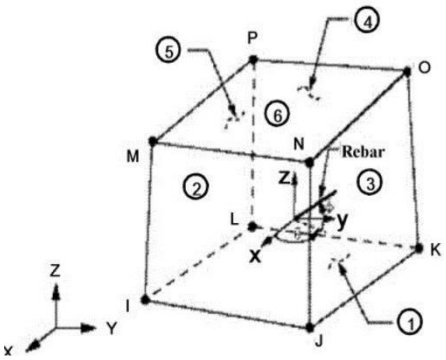

Fig. 6 Solid65-3D solids modeling, ANSYS (2005)

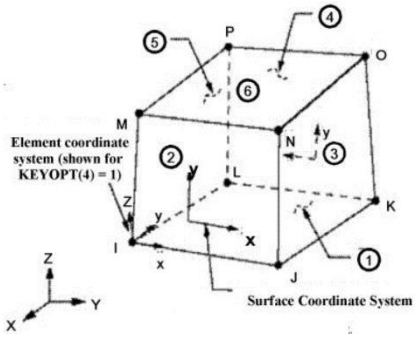

Fig. 7 Solid45-3D solids Modeling, ANSYS (2005)

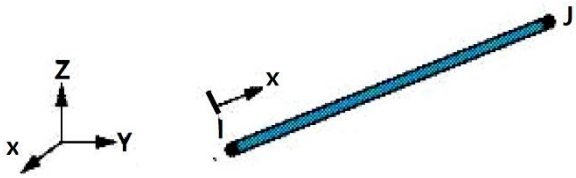

Fig. 8 Link8-3D spar modeling, ANSYS (2005)

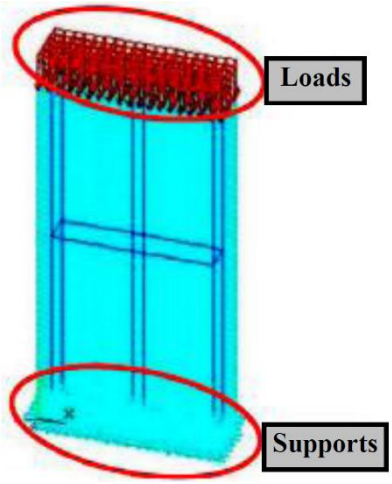

Fig. 9 FE simulation of the tested wall W10

2.3 Mechanical properties of mixes

All mixes were performed using mechanical mixer. For all mixes, the constituent materials were first dry mixed; then, the mix water was added during mixing. Mechanical compaction was applied for all specimens using a mechanical vibrator. The values of the average compressive strength of the concrete and mortar are shown in Table 2.

2.4 Preparation and testing of test specimens

The cages of the twelve walls using steel bars combined with metallic and non metallic meshes were prepared. The molds used for casting the test specimens were placed on a vibrating table to assure good compaction of ferrocement mortar as shown in Fig. 5. The wooden molds were disassembled on the next day and the specimen was weighed. The specimens were placed in the curing room for 28 days.

3. Finite element analysis

Nonlinear finite element analysis; (NLFEA) was carried out to investigate the behavior of the reinforced concrete walls using innovative composites specimens employing ANSYS-10.0 Software (2005). The investigated behavior includes the cracks pattern, the ultimate load and the load-vertical displacement response of the test specimens. Measurements were taken on central 200 mm length of the wall, same as laboratory measurements. In addition, extensive non linear finite elements analysis had been conducted to investigate in deep the behavior of the RC walls reinforced by innovative composites.

Solid65 elements were used for modeling mortar and wire steel meshes, such as expanded, welded, tensar, etc., using smeared rebar model method. The reinforcement of all these types of meshes was defined by using the real constants of solid65 element. Each element is defined by eight nodes. Each node has three degrees of freedom (translations in the nodal x, y, and z directions). This element has one solid material and up to three rebar materials in the three directions. The solid material is used to model the mortar. The rebar capability is used for modeling wire mesh. The wire mesh is specified by its material, volume ratio and orientation angles as illustrated in Fig. 6. This element has the ability of cracking (in the three orthogonal directions), crushing, plastic deformation, and creep as discussed by Hoque (2006), Singh (2006), Shaheen *et al.* (2013).

An eight-node solid element, Solid 45, was used to model the steel plates under the load. The element is defined with eight nodes having three degrees of freedom at each node in the nodal x, y, and z directions. The geometry and node locations for this element type are shown in Fig. 7. Steel bars and stirrups were modeled by link8 elements. Link8 is a uniaxial tension-compression element with three degrees of freedom at each node: translations in the nodal x, y, and z directions. Plasticity, creep, swelling, stress stiffening, and large deflection capabilities are included. A schematic of the element was shown in Fig. 8.

Each support was presented by 114-hinged supports. The load was concentrated at the top end of the analyzed walls as demonstrated in Fig. 9.

The material of the mortar is defined by the compressive, tensile strength of concrete after 28 days, the modulus of elasticity and the multi-linear isotropic stress-

Table 3 First crack and ultimate load results for all test specimens

Designation	Volume Fraction (%)	First Crack load (kN)	Ultimate Load (kN)	Load-Carrying Capacity Enhancement (%)
*W*1	1.5054	436.32	1149.40	0.00
*W*2	0.4665	814.46	1159.51	0.88
*W*3	0.9240	891.70	1268.36	10.35
*W*4	0.9330	884.82	1349.05	17.37
*W*5	1.9809	909.07	1420.43	23.58
*W*6	0.3710	972.10	1621.46	41.07
*W*7	1.4189	1283.14	1868.69	62.58
*W*8	0.7420	1207.15	1843.06	60.35
*W*9	1.7899	1401.40	1946.97	69.39
*W*10	1.7519	905.14	1221.47	6.27
*W*11	1.4749	779.79	871.36	-24.19 (no enhancement)
*W*12	2.6039	933.33	1061.36	-7.66 (no enhancement)

strain curve. The modulus of elasticity of concrete and stress-strain curve were employed the Egyptian Code (2007). The modulus of elasticity of concrete (E_c in MPa) can be calculated from Eq. (3) by considering the compressive strength of concrete after 28 days (F_{cu} in MPa).

The multi-linear isotropic stress- strain curve for the concrete can be computed by Eq. (4). The modulus of elasticity of concrete is considered as 14 GPa. The steel and the wire meshes were defined by the yield stress and the modulus of elasticity as illustrated in the material properties section.

$$E_c = 4400\sqrt{F_{cu}} \tag{3}$$

$$stress = \frac{E_c \varepsilon}{1+(\varepsilon/\varepsilon_o)^2} \tag{4}$$

$$\varepsilon_o = \frac{2F_{cu}}{E_c} \tag{5}$$

4. Results and discussion

4.1 Experimental results

In what follows the performance of the RC walls reinforced with different innovative composite materials is presented and discussed. The compression behavior was investigated including the load-carrying capacity, the cracking pattern, the failure mode and finally the specimen's deformation and strains.

All test specimens were tested under concentric compression loadings and readings for deformation over a gauge length of 200 mm versus the applied load were

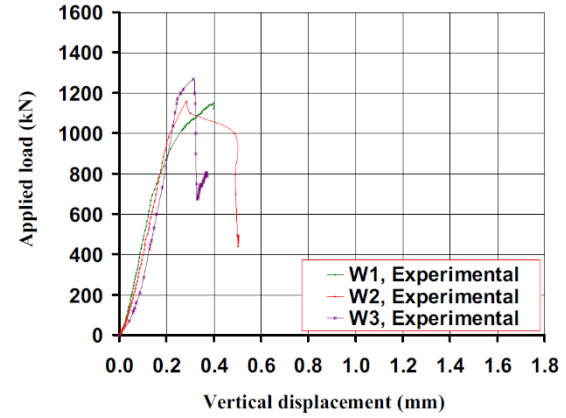

(a) Series *W*1, *W*2, and *W*3

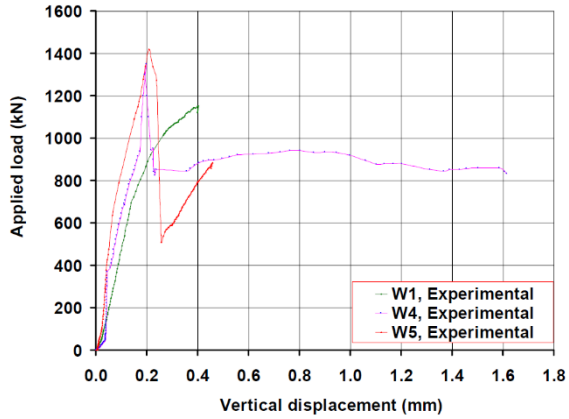

(b) Series *W*1, *W*4, and *W*5

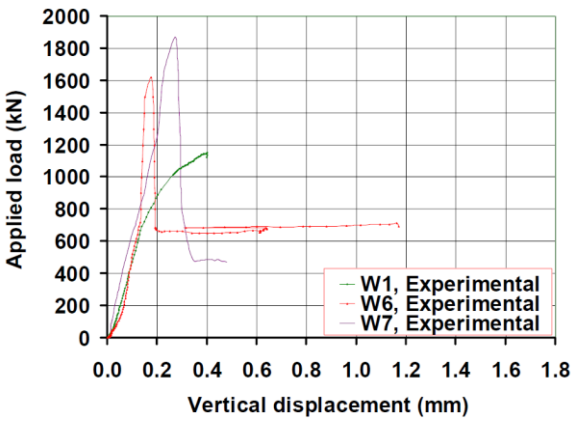

(c) Series *W*1, *W*6, and *W*7

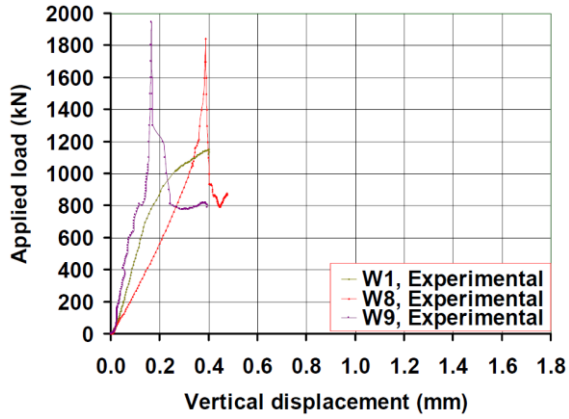

(d) Series *W*1, *W*8, and *W*9

Fig. 10 Load-vertical displacement curves for series *W*1 to *W*12

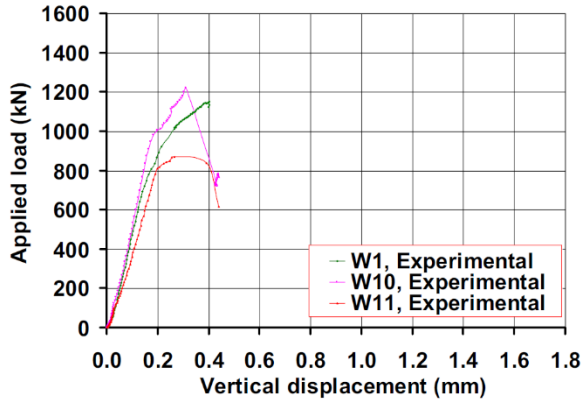

(e) Series $W1$, $W10$, and $W11$

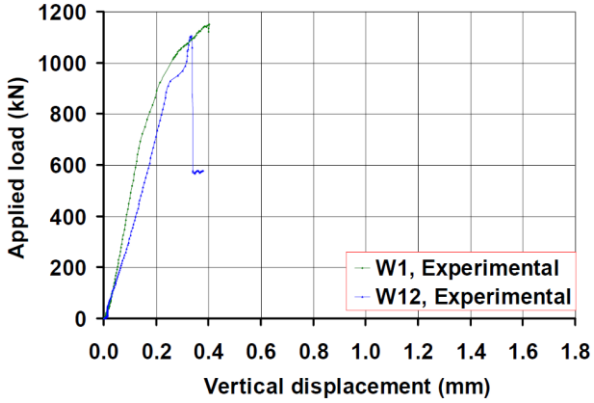

(f) Series $W1$ and $W12$

Fig. 10 Continued

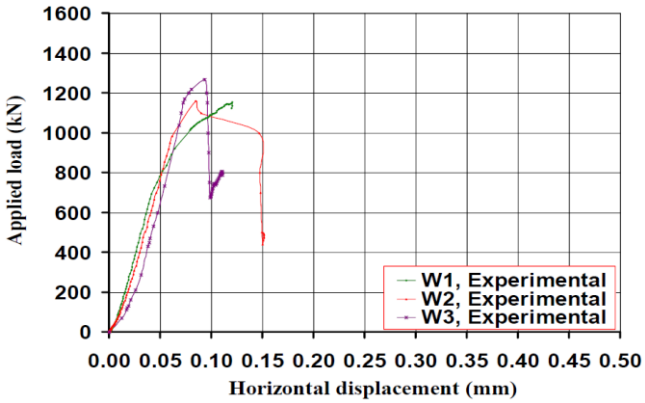

(a) Series $W1$, $W2$, and $W3$

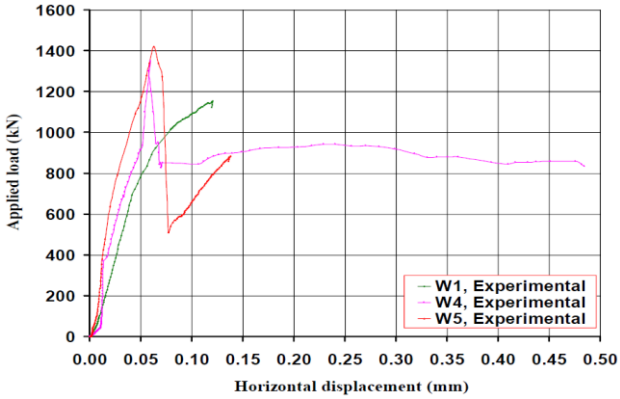

(b) Series $W1$, $W4$, and $W5$

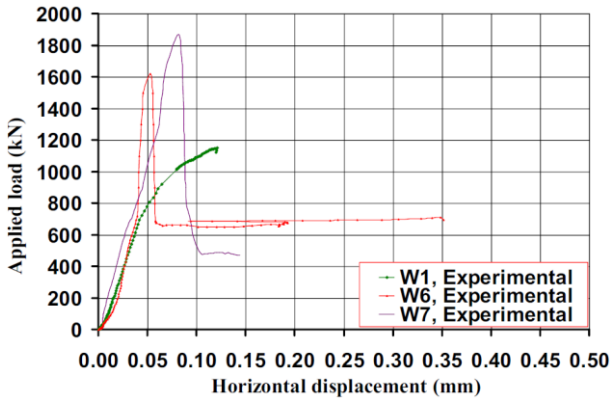

(c) Series $W1$, $W6$, and $W7$

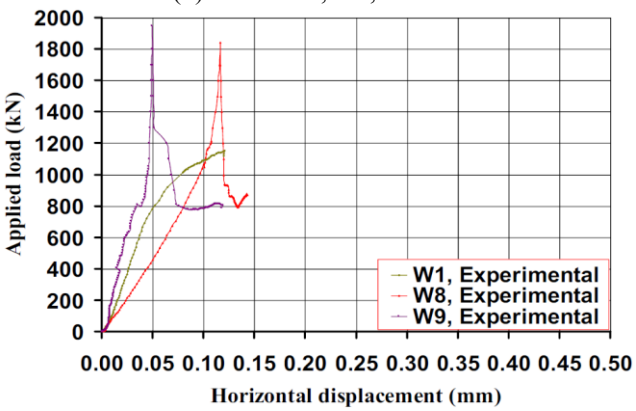

(d) Series $W1$, $W8$, and $W9$

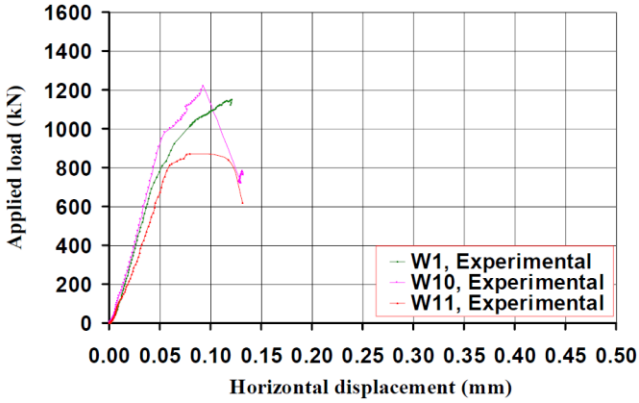

(e) Series $W1$, $W10$, and $W11$

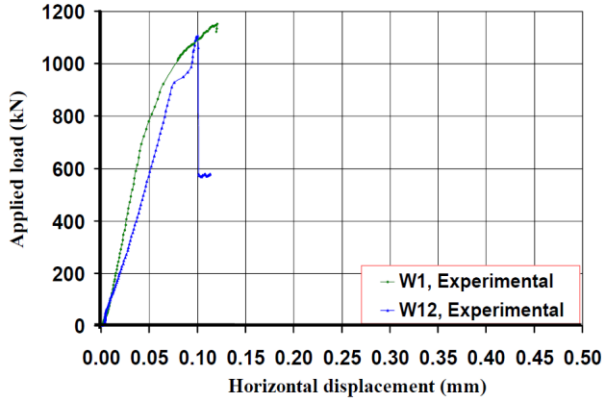

(f) Series $W1$ and $W12$

Fig. 11 Load-horizontal-displacement curves for series $W1$ to $W12$

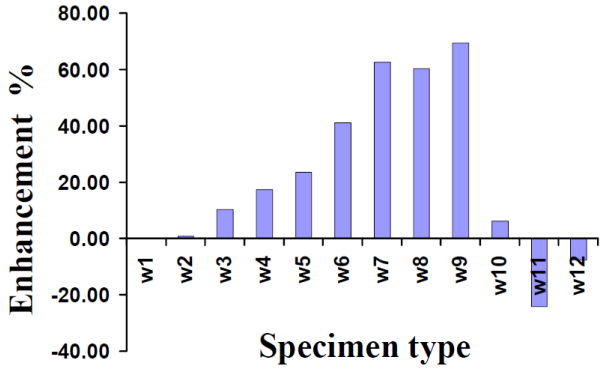

Fig. 12 Enhancement percentage in experimental carrying capacity

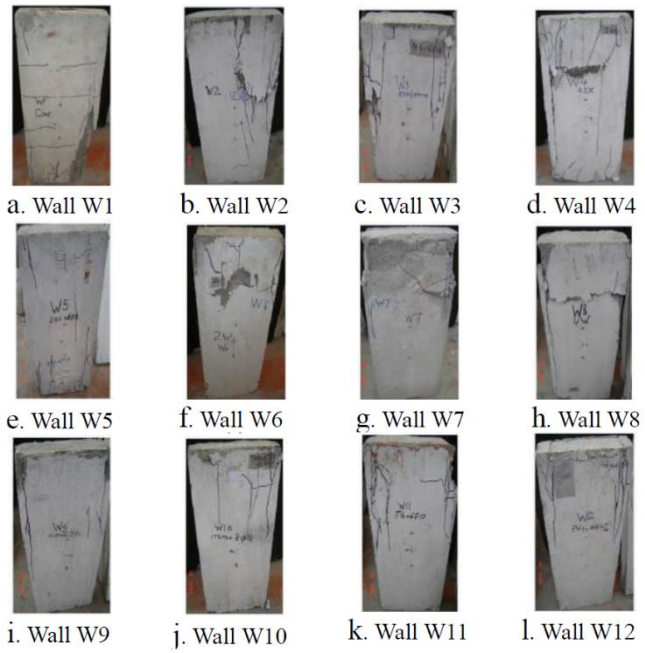

Fig. 13 Cracking patterns for all test specimens

recorded using data acquisition system to construct load-deformation curves.

4.1.1 Ultimate capacity

Table 3 illustrates first crack and ultimate loads for all the tested walls. According to the results, the failure load of specimen W9 was 1946.97 kN, indicating biggest significant enhancement in ultimate capacity. In addition, the effect of using welded wire mesh is more effective in enhancing the ultimate capacity than the other various types of metallic and non metallic mesh reinforcement.

Figs. 10 (a) to (f) and 11 (a) to (f) show the comparisons of load-vertical displacement and load-horizontal displacement curves for all tested specimens with respect to the control specimen *W*1. In addition, Fig. 12 indicates the enhancement percentage in experimental carrying load capacity for different specimens.

4.1.2 Cracking

The first cracks in control specimen W1 started at load of 436.32 kN at the wall head under the point of load

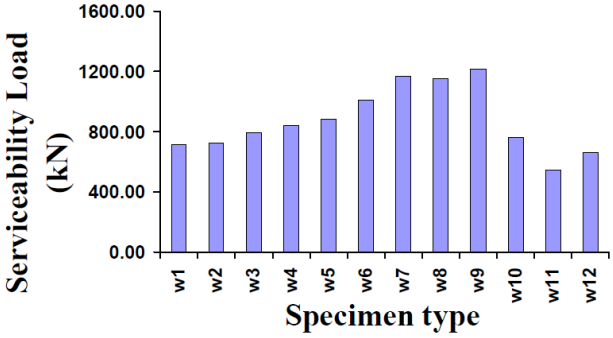

Fig. 14 Serviceability loads in function of tested specimen type

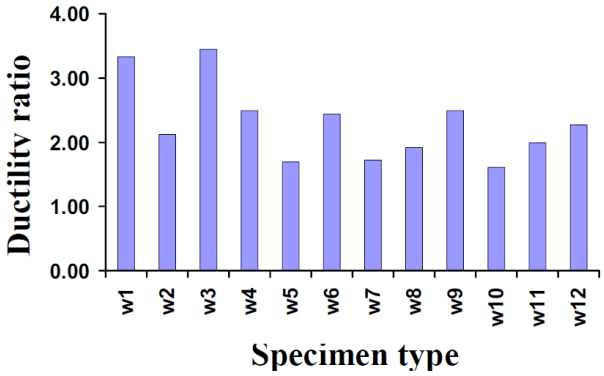

Fig. 15 Ductility ratios in function of tested specimen type

concentration, and then propagated suddenly at the maximum load of 1149.40 kN. After this, the load decreases and the cracks increased showing the failure of wall.

For specimens *W*9, the recorded first crack load showed maximum increased value about 221.19%, compared to the control specimen. This indicates the capability of the welded wire mesh than the other techniques.

Generally, the cracks for all tested walls started at later stage of loading indicating better confinement and better serviceability. However, the ultimate strength increased and the cracks slightly increased in length and width to different extent, as shown in Fig. 13 (a) to (l) and Table 4.

4.1.3 Modes of failure

The control specimen wall failed in a mode of compression failure accompanied with local crushing and spalling of the concrete cover. For the other series of the tested specimens, near failure the load reach the maximum value and after this value the load decreased up to 70% to 50% of the maximum load with increasing the descending part of load displacement curves. This indicates the increases of the service load which represent the safe line in using the structures as shown in Table 4 and Fig. 14.

4.1.4 Ductility and energy absorption

Ductility ratio was defined as the ratio of the maximum deformation at ultimate load to that at the first crack load, while energy absorption was defined as the area under the load-deformation curve up to failure. Table 4 shows the values of the ductility ratios and energy absorption of all the tested walls. Progressive increase of energy absorption with

Table 4 Deformation characteristics of tested walls

Designation	Volume Fraction (%)	1st crack load (P_{FC}, kN)	Serviceability load (*) (P_{ser}, kN)	Ultimate load (P_{ult}, kN)	Ductility ratio	Energy Absorption (kN.mm)
*W*1	1.5054	436.32	718.28	1149.40	3.33	363.00
*W*2	0.4665	814.46	724.60	1159.51	2.13	468.00
*W*3	0.9240	891.70	792.63	1268.36	3.45	420.00
*W*4	0.9330	884.82	843.06	1349.05	2.50	819.00
*W*5	1.9809	909.07	887.67	1420.43	1.69	630.00
*W*6	0.3710	972.10	1013.31	1621.46	2.44	754.00
*W*7	1.4189	1283.14	1167.83	1868.69	1.72	562.00
*W*8	0.7420	1207.15	1151.81	1843.06	1.92	637.00
*W*9	1.7899	1401.40	1216.76	1946.97	2.50	595.00
*W*10	1.7519	905.14	763.32	1221.47	1.61	515.00
*W*11	1.4749	779.79	544.50	871.36	2.00	470.00
*W*12	2.6039	933.33	663.25	1061.36	2.27	334.00

(*) $P_{ser} = \frac{(P_{ult} - 1.4 * D.L.)}{1.6}, D.L. = own \quad weight \quad of \quad wall.$

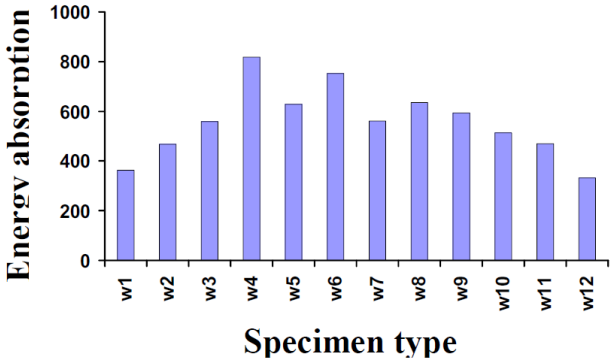

Fig. 16 Energy absorption in function of tested specimen type

volume fraction percentage was observed. Fig. 15 shows comparison of the ductility ratio values for all tested specimens. It is observed that the wall *W*3, which use one layer of expanded steel mesh instead of the traditional reinforcement (steel bars and stirrups), with six longitudinal steel bars, each has a diameter 10 mm, has a maximum ductility ratio.

Fig. 16 shows comparison of the energy absorption values for all tested specimens. It is cleared that the wall W4, which use two layers expanded steel mesh, has maximum energy absorption.

It can be concluded that using these innovative composites enhanced the behavior of failure by increasing the energy absorption values.

It can be state that it delayed the appearance of the first cracks and increased the service load capacity. In addition, it developed with high ultimate loads, crack resistance, better deformation characteristics, high durability, high ductility and energy absorption properties, which are very useful for dynamic applications.

4.1.5 Compressive strain

Figs. 17 (a) to (f) show the comparison of compressive strain curves for all tested specimens with respect to the control specimen *W*1.

Table 5 shows compressive strains at first crack and ultimate loads of all the tested walls, while Figs. 18 and 19 show comparison of the compressive strains at first crack and ultimate loads respectively.

Table 5 Compressive strain at 1st crack and ultimate loads of tested walls

Designation	Volume Fraction (%)	Compressive strain at 1st crack load ($\times 10^{-4}$)	Compressive strain at ultimate load ($\times 10^{-4}$)
*W*1	1.5054	13.10	20.00
*W*2	0.4665	8.46	14.10
*W*3	0.9240	10.89	15.56
*W*4	0.9330	6.40	10.00
*W*5	1.9809	6.60	10.00
*W*6	0.3710	4.24	7.57
*W*7	1.4189	9.36	13.56
*W*8	0.7420	12.19	19.35
*W*9	1.7899	4.54	8.25
*W*10	1.7519	8.96	15.45
*W*11	1.4749	7.66	13.20
*W*12	2.6039	11.52	16.70

It can be concluded that the specimen *W*3, which reinforced with one layer expanded steel mesh, with six longitudinal steel bars, each has a diameter 10 mm, has a maximum compressive strain at first and ultimate loads respectively. This is due to this tested specimen has a lowest amount of reinforcement, in comparison to the other walls.

4.2 Comparison between experimental and FE simulation results

The comparison between experimental and FE simulation results; include 1st crack load, serviceability load, ultimate load, cracking patterns, curves of load-vertical displacement, and ductility ratio.

4.2.1 Ultimate load carrying capacity

Good agreement between the nonlinear finite element analysis (NLFEA) predictions and the recorded load-carrying capacity is shown in Fig. 20 and Table 6. For the control specimen *W*1, the analytical ultimate load to the experimental load; $P_{ult(NLFEA)}/P_{ult(EXP.)}$ was equals to 1.04.

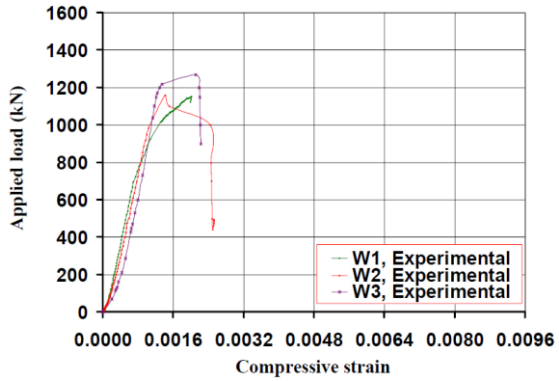

(a) Series *W*1, *W*2, and *W*3

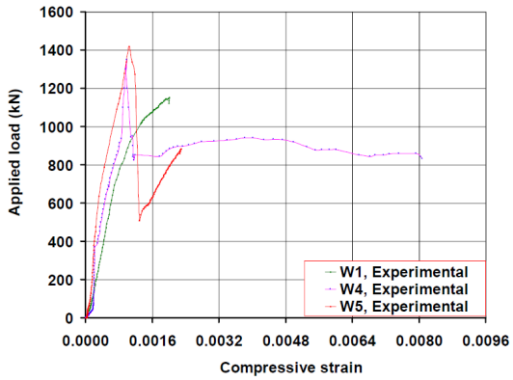

(b) Series *W*1, *W*4, and *W*5

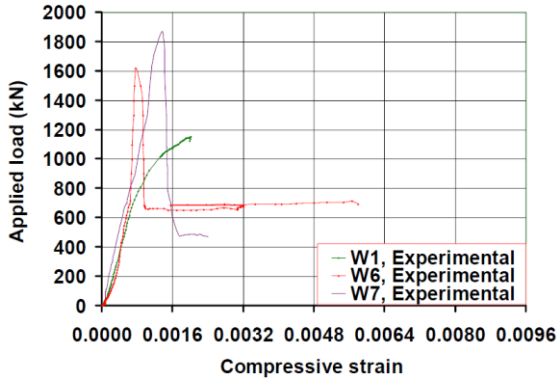

(c) Series *W*1, *W*6, and *W*7

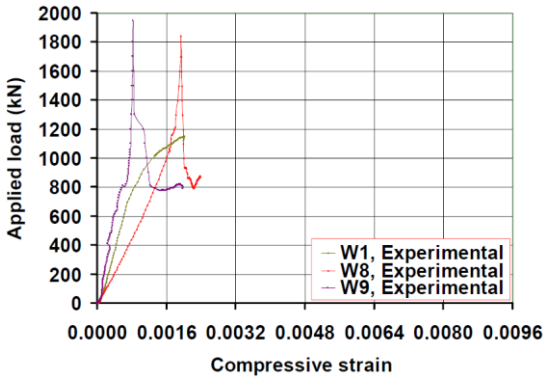

(d) Series *W*1, *W*8, and *W*9

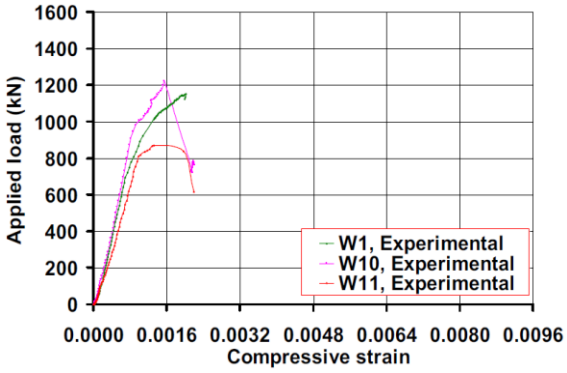

(e) Series *W*1, *W*10, and *W*11

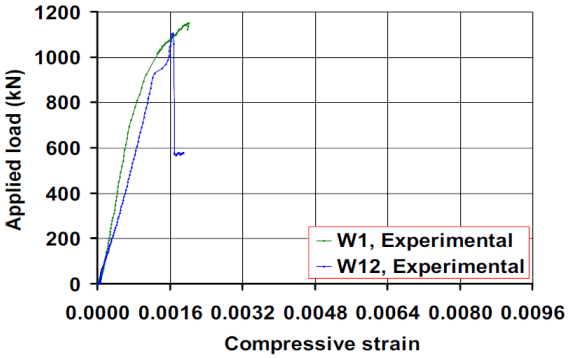

(f) Series *W*1 and *W*12

Fig. 17 Compressive strain in function of tested specimen type

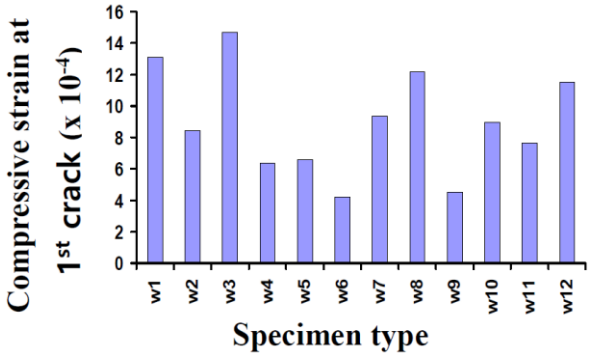

Fig. 18 Compressive strain in function of tested specimen type at 1st crack load

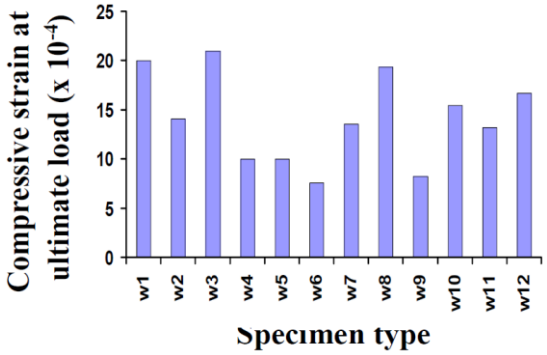

Fig. 19 Compressive strain in function of tested specimen type at ultimate load

For other specimens, this ratio ranges between 1.24 and 0.84 with a mean value of 1.04. The analysis reflected the strengthening significance. The comparison between the experimental and the analytical enhancement values in

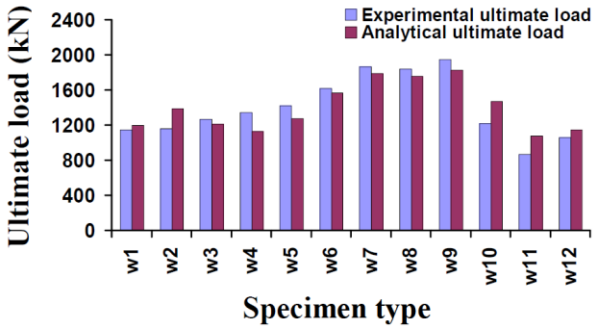

Fig. 20 Failure load of selected models with varying wall type

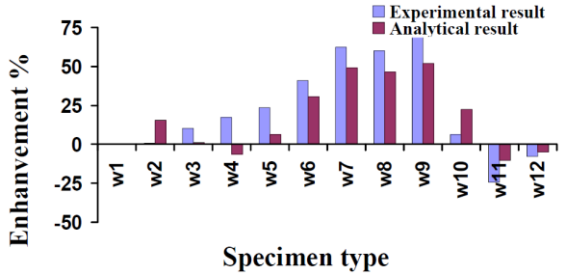

Fig. 21 Enhancement percentage in experimental and analytical carrying capacity

Table 6 Comparison of the experimental and FE 1st crack and ultimate loads for tested walls

Designation	Initiation of crack P_{FC} (kN)		Ultimate load P_{ult} (kN)		$P_{FC\,(NLFEA)}/P_{FC\,(EXP)}$	$P_{ult\,(NLFEA)}/P_{ult(EXP)}$
	EXP.	NLFEA	EXP.	NLFEA		
*W*1	436.32	510.36	1149.40	1201.06	1.17	1.04
*W*2	814.46	577.08	1159.51	1390.90	0.71	1.20
*W*3	891.70	480.03	1268.36	1215.00	0.54	0.96
*W*4	884.82	422.11	1349.05	1128.44	0.48	0.84
*W*5	909.07	450.14	1420.43	1276.97	0.50	0.90
*W*6	972.10	486.08	1621.46	1569.00	0.50	0.97
*W*7	1283.14	467.88	1868.69	1793.00	0.36	0.96
*W*8	1207.15	461.84	1843.06	1760.00	0.38	0.95
*W*9	1401.40	469.78	1946.97	1827.00	0.34	0.94
*W*10	905.14	592.77	1221.47	1470.87	0.65	1.20
*W*11	779.79	630.56	871.36	1080.45	0.81	1.24
*W*12	933.33	502.27	1061.36	1147.00	0.54	1.08

ultimate load capacity P_u was as shown in Fig. 21.

4.2.2 Cracking behavior

The cracking was initiated at early loading stage in the concrete elements modeling the loaded face of the wall nearby the supporting of walls as shown in Fig. 22.

Referring to Table 6, the experimental cracking capacity is shown to be vary from 436.32 kN for specimen *W*1, and 1401.40 kN for specimen *W*9, being somewhat independent on the reinforcing characteristics. This early stage of crack loading is due to the unseen micro cracks in experimental test. The cracking load, as such, is quite below the experimental cracking capacity. The ratio of the analytical cracking load to the experimental load. $P_{FC(NLFEA)}/P_{FC(EXP)}$ is

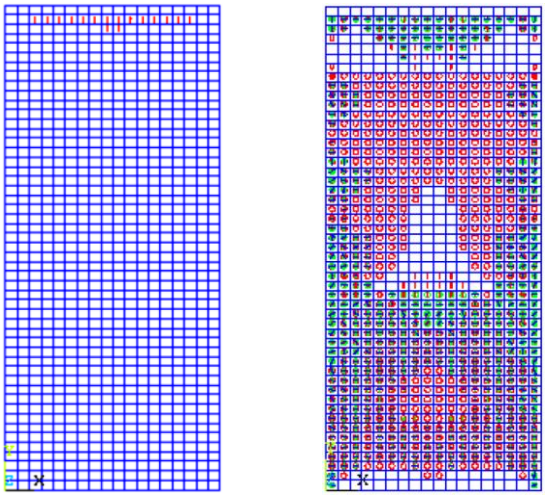

(a) 1st crack (b) all cracks

Fig. 22 First and all cracks of control specimen

shown to be ranged from 0.34 to 1.17 with a mean value of 0.76 as illustrated in Table 6.

This is may be justified as the NLFEA predictions represent the micro-cracking stage which precedes the visible cracking stage. Moreover, the innovative composites materials might have concealed the micro cracks developed underneath in the experiments.

On the other hand, the cracking patterns at each load increment revealed that propagation of the cracks for all specimens was slightly different with respect to the experimental crack pattern.

This is due to the accuracy of the non linear finite element program in determined the micro cracks and wide cracks, and reflected the significance of the reinforcing method on the cracking patterns as shown in Table 6. The comparison of the crack patterns for the experimental and the analytical cases is illustrated as shown in Fig. 23 (a) to (l).

4.2.3 Deformation characteristics

Figs. 24 (a) to (f) and 25 (a) to (f) present the load-vertical displacement curves; and also the load-horizontal displacement curves, as obtained from the experimental and theoretical approaches for the all test composite walls. Good agreement is observed between the theoretical and experimental results as shown.

Figs. 26 and 27 show the comparison of the compressive strains for the experimental and the analytical cases at 1st crack and ultimate loads respectively. It can be concluded that the FE simulations give accurate results in comparing with the experimental results. In addition, the analytical compressive strain results experience greater than the experimental results by a mean value of 14% as shown.

5. Parametric study

To further improve the understanding of the mechanical behavior of RC walls reinforced with composite materials, parametric studies were performed to investigate the impact

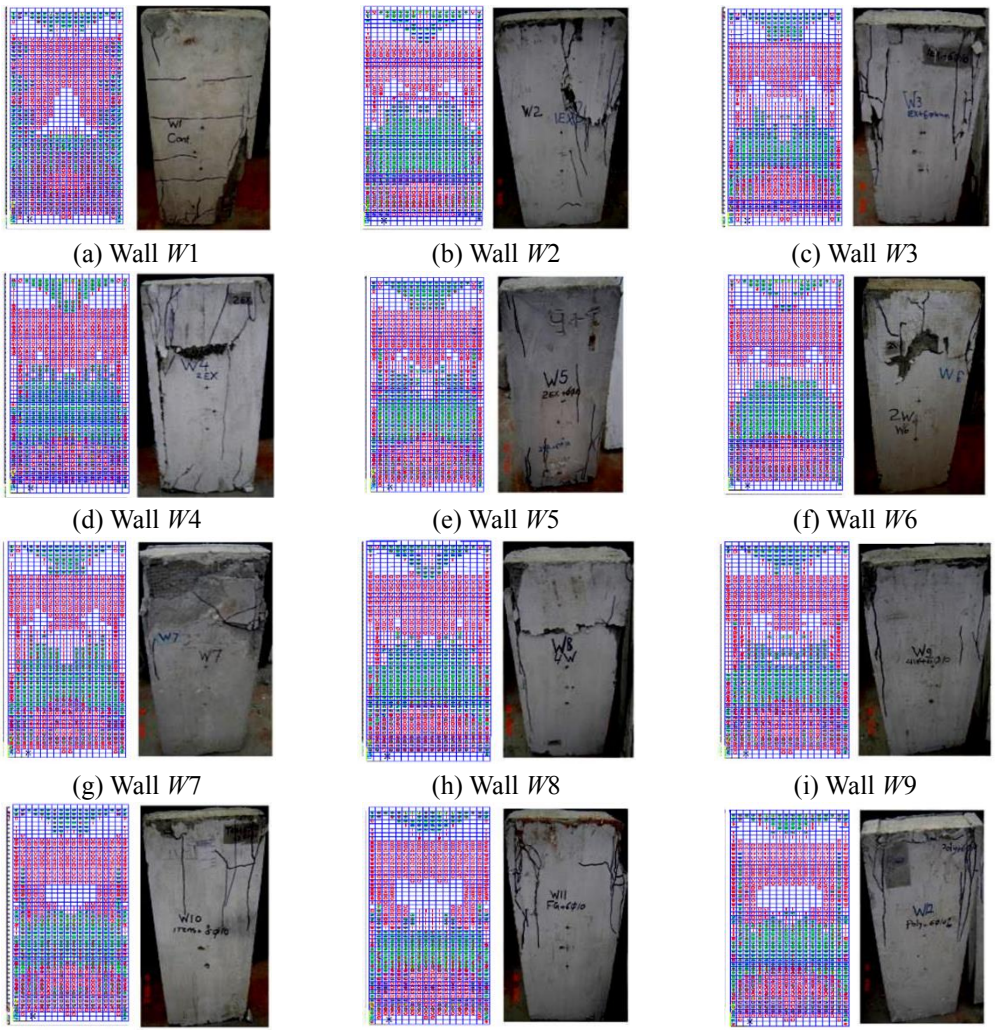

(a) Wall *W*1 (b) Wall *W*2 (c) Wall *W*3

(d) Wall *W*4 (e) Wall *W*5 (f) Wall *W*6

(g) Wall *W*7 (h) Wall *W*8 (i) Wall *W*9

(j) Wall *W*10 (k) Wall *W*11 (l) Wall *W*12

Fig. 23 Experimental and analytical crack patterns for all walls

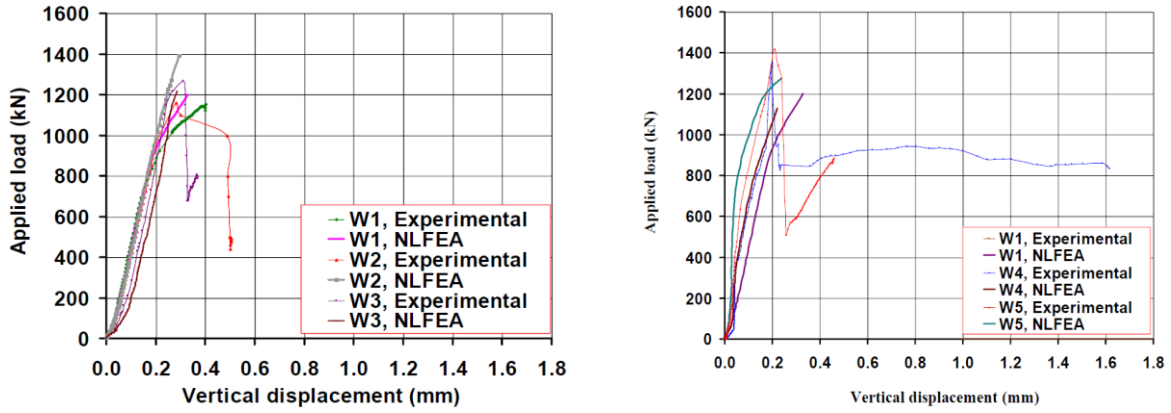

(a) Series *W*1, *W*2, and *W*3 (b) Series *W*1, *W*4, and *W*5

Fig. 24 Curve applied load in function of vertical displacement of experimental and proposed models for series *W*1 to *W*12

of the increase of the wall dimensions, upon the strength capacity of the models having ferrocement reinforcement.

The study was conducted on three proposed models. The first model has cross section dimensions of 450 mm×150 mm and length of 1500 mm. The second has cross section dimensions of 450 mm×200 mm and has length of 2000 mm, while the third model has cross section dimensions of 450 mm×250 mm and has length of 2500 mm.

Fig. 28 compares the results obtained for the ultimate load values. It has to be observed that in case of an increase of the wall width by an amount of 50%, the FE ultimate load increase by a mean value of 58%, according to the

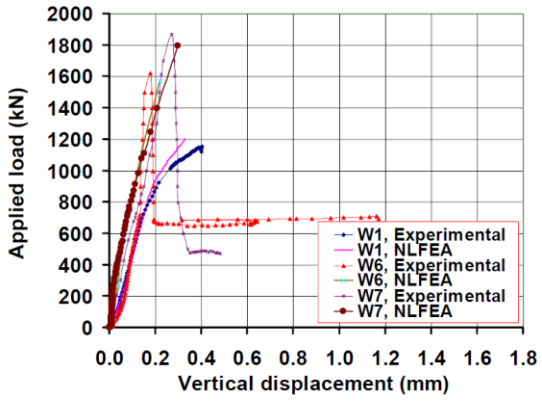

(c) Series *W*1, *W*6, and *W*7

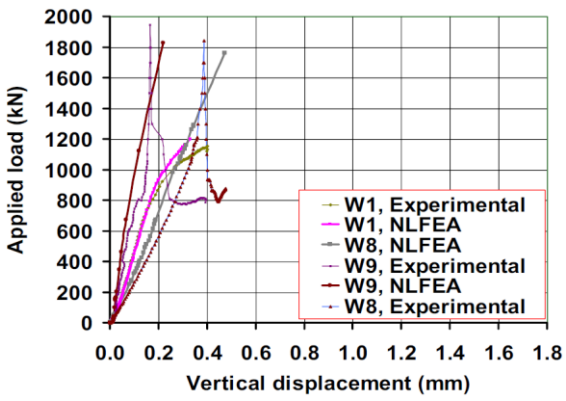

(d) Series *W*1, *W*8, and *W*9

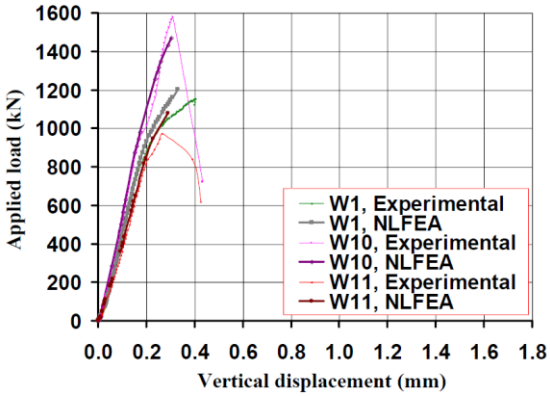

(e) Series *W*1, *W*10, and *W*11

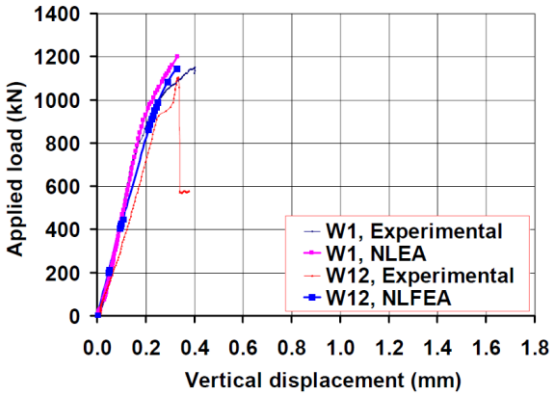

(f) Series *W*1 and *W*12

Fig. 24 Continued

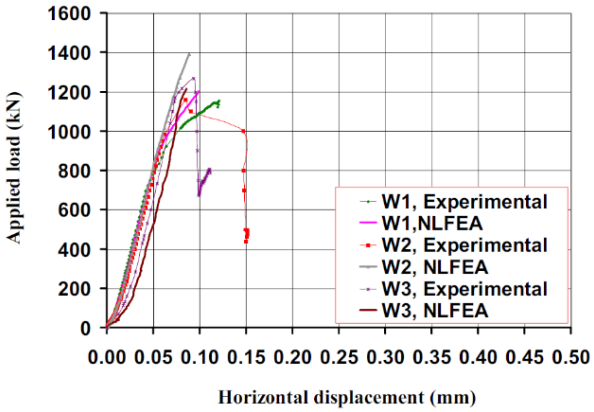

(a) Series *W*1, *W*2, and *W*3

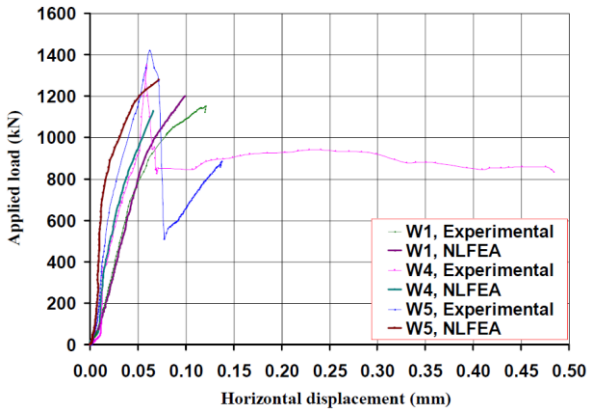

(b) Series *W*1, *W*4, and *W*5

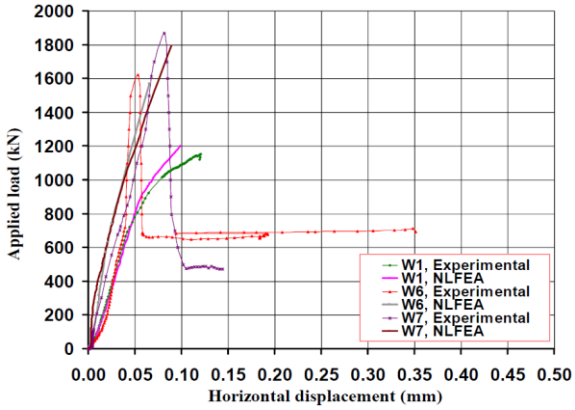

(c) Series *W*1, *W*6, and *W*7

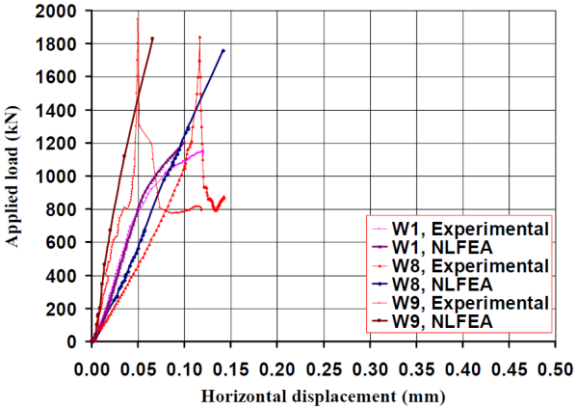

(d) Series *W*1, *W*8, and *W*9

Fig. 25 Curve applied load in function of horizontal displacement of experimental and proposed models for series *W*1 to *W*12

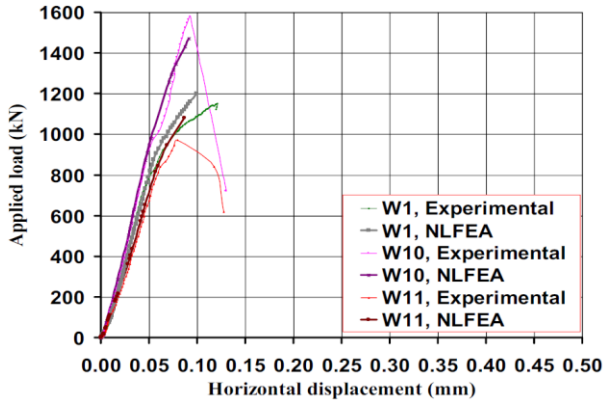

(e) Series *W*1, *W*10, and *W*11

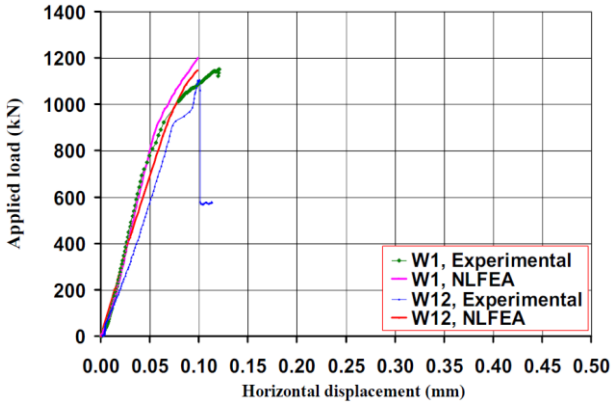

(f) Series *W*1 and *W*12

Fig. 25 Continued

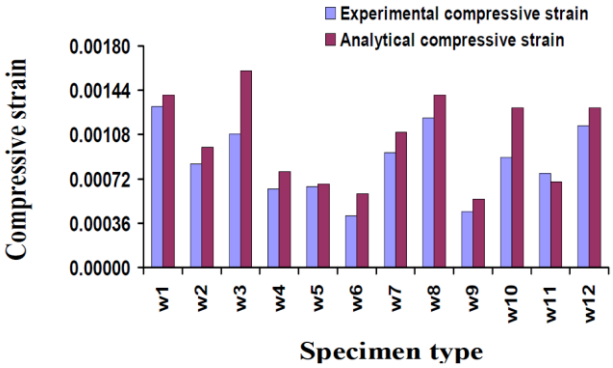

Fig. 26 Compressive strain in function of specimen type at 1st crack

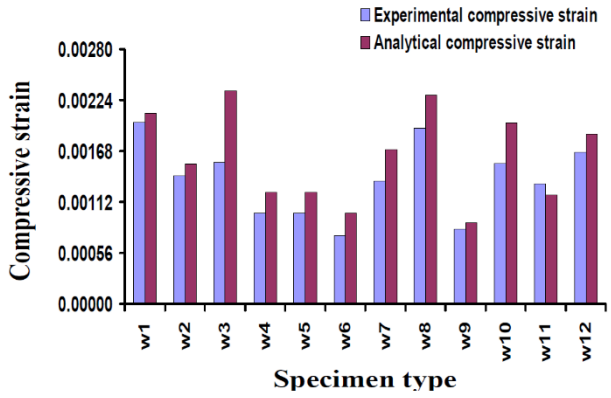

Fig. 27 Compressive strain in function of specimen type at ultimate load

reinforcement type of composite wall.

6. Conclusions

This research aimed to compare the performance of the ferrocement RC walls reinforced with intentive composite materials, such as welded and expanded steel mesh, fiber glass and tensar mesh, with the conventional reinforced concrete walls. The studied variables were the type of reinforcing materials, the number of mesh layers and volume fraction of reinforcement.

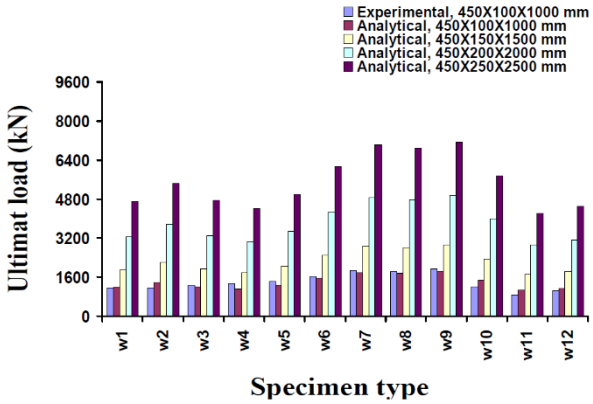

Fig. 28 Ultimate load in function of specimen type with varying wall size

Based on the results and observations of the experimental and the analytical study presented in this study, and considering the relatively high variability and the statistical pattern of data, the following conclusions can be drawn:

1. Irrespective of the steel mesh type, expanded or welded, ferrocement RC wall specimens tested under axial compression loadings exhibit superior ultimate loads, enhance the energy absorbing capacity of the specimens, delay the cracks propagation, compared to the control one.
2. Changing steel mesh types, expanded or welded have much effect on ultimate loads under axial compression loading. The strength gained by employing welded steel mesh as reinforcement was about 58% compared to the conventionally RC walls, while the same value was 13% by employing expanded steel mesh. As a result, there is higher strength gain of specimens reinforced with welded steel mesh about 40% compared with those reinforced with expanded steel mesh, illustrating the preferable of using welded steel meshes in reinforcing the RC walls.
3. Increasing the number of ferrocement layers in reinforcing RC walls led to improving performance for such specimens compared to the traditionally reinforced increased one, in terms of attaining higher ultimate load and displacement until failure.

5. Wrapping RC walls with tensar mesh showed higher ultimate load compared with those reinforced with fiber glass or polyethylene mesh with the same number of layers, confirming the advantage of using tensar mesh as non metallic reinforcement.
6. Reinforcing RC walls with fiber glass mesh, it was observed that longitudinal cracks were occurred on the sides of the specimens at 72% of that of respective ultimate load. This could be attributed due to the effect of low strength of glass mesh used as non metallic reinforcement.
7. Finite element model can be used to investigate the mechanical behavior of ferrocement RC walls reinforced with composite material, leading to a good agreement when comparing to available full-scale test data.
8. The comparison of the crack patterns obtained by the FE and experimental models leads to an identical crack propagation for the two approaches up to failure. The inclination of the failure surfaces and the concentration of cracks of all walls were the same in both patterns.
9. An increase in the FE strength capacity mean values of 17.6% compared to the experimentally available data was concluded, leading to a good agreement between them.
10. It has to be observed that in case of an increase of the wall width by an amount of 50%, the FE ultimate load increase by a mean value of 58%, according to the reinforcement type of the composite wall.

References

Abdel-Naby, A. (2006), "Development of ferrocement U-shaped beams infilled with core materials", M.S. Thesis, American University in Cairo, Egypt.

Al-Rifiaie, W.N. and A-Aziz, A. (1995), "Thin ferrocement bearing walls", *J. Ferroce.*, **25**(3), 247-259.

Amin, M.A., Alam, M.K., Rahman, M.M., Rahman, M.S. and Islam, M.A. (2015), "Study of double layer wire mesh ferrocement plate using neutron imaging technique", *Int. J. Adv. Res. Technol.*, **4**(7), 83-92.

ANSYS (2005), Engineering Analysis System User's Manual, Vol. 1&2, and Theoretical Manual, Revision 8.0, Swanson Analysis System Inc., Houston, Pennsylvani.

ASTM C III6/C III6M (2015), Standard Specification for Fiber-Reinforced Concrete, ASTM International, 100 Barr Harbor Drive, PO Box C700, West Conshohocken, PA, 19428-2959 USA.

Basunbul, I.A., Saleem, M. and Al-Sulaimani. G.J. (1990), "Structural behavior of ferrocement load bearing walls panels", *J. Ferroce.*, **20**(1), 1-9.

Bezbradica, M. (2015), "Analysis of ferrocement and textile reinforced concrete for shell structures", M.S. Thesis, Lund University, Sweden.

Deshpande, N. and Shirsath, M. (2016), "Comparative study between bamboo reinforced and conventional ferrocement panels", *Int. J. Res. Publ Eng. Technol.*, **2**(7), 6-9.

Fahmy, E.H. (2004), "Ferrocement sandwich and cored panels for floor and wall construction", *Proceedings of the 29th Conference on our World in Concrete & Structures*, Singapore.

Fahmy, E.H., Shaheen, Y.B. and Abou Zeid, M.N. (2004), "Development of ferrocement panels for floor and wall construction", *Proceedings of the 5th Structural Specialty Conference of the Canadian Society for Civil Engineering*, 1-10.

Fahmy, E.H., Shaheen, Y.B., Abou Zeid, M.N. and Gaafar, H. (2004), "Ferrocement sandwich and cored panels for floor and wall construction", *Proceedings of the 29th Conference on Our World in Concrete & Structures*, 245-252.

Gaafar, H.M. (2004), "Ferrocement sandwich and hollow core panels for floor and wall construction", MS Thesis, American University in Cairo, Egypt.

Grija, S., Sivakumar, P., Lakshmikandhan, K.N., Ravichandran, R. and Karthikeyan, B. (2014), "Novel ferrocement light weight wall panels", *Int. J. Appl. Eng. Res.*, **9**(18), 4645-4657.

Hoque, M. (2006), "3D nonlinear mixed finite-element analysis of RC beams and plates with and without FRP reinforcement", M.Sc. Thesis, University of Manitoba, Winnipeg, Manitoba, Canada.

Housing and Building national research Center (2007), The Egyptian Code for Design and Construction of Concrete Structures, ECP 203-2007, Ministry of Housing, Utilities and Urban Communities, Giza, Egypt.

IFS Commitee 10 (2001), Ferrocement Model Code: Building Code Recommendations for Ferrocement, IFS 10-01, International Ferrocement Society, Asian Institute of Technology, Bangkok, Thailand.

Lakshmikandhan, K.N., Harshavardhan, B.S., Prabakar, J. and Saibabu, S. (2017), "Investigation on wall panel sandwiched with lightweight concrete", *IOP Conf. Ser.: Mater. Sci. Eng.*, **225**(1), 012275.

Lakshmikandhan1, K.N., Sivakumar, P., Ravichandran, R., Sivasubramanian, K. and Saibabu, S. (2015), "Development and testing of novel ferrocement wall panels", *Int. J. Res. Eng. Technol.*, **4**(13), 500-509.

Memon, N.A., Sumadi, S.R. and Ramli, M. (2004), "Strength and behavior of light weight ferrocement-aerated concrete sandwich blocks", MS Thesis, American University in Cairo, Egypt.

Rashid, M.H., Alam, Z., Mahmud, F. and Anita, M.S. (2019), "Durability and performance of ferrocement infill wall panel", *Civil Eng. J.*, **5**(6), 1205-1213.

Shaaban, I.G. and Seoud, O.A. (2018), "Experimental behavior of full-scale exterior beam-column space joints retrofitted by ferrocement layers under cyclic loading", *Case Stud. Constr. Mater.*, **8**, 61-78. https://doi.org/10.1016/j.cscm.2017.11.002.

Shaaban, I.G., Shaheen, Y.B.I., Elsayed, E.L., Kamal, O.A. and Adesina, P.A. (2018), "Experimental behavior of full-scale exterior beam-column space joints retrofitted by ferrocement layers under cyclic loading", *Constr. Build. Mater.*, **171**, 802-816. https://doi.org/10.1016/j.cscm.2017.11.002.

Shaheen, Y.B.I., Eltaly, B. and Kameel, M. (2013), "Experimental and Analytical Investigation of Ferrocement Water pipe", *J. Civil Eng. Constr. Tech.*, **4**(4), 157-167.

Shaheen, Y.B.I., Mohamed, A.M. and Mohamed, H.R. (2016), "Structural performance of ribbed ferrocement plates reinforced with composite materials", *Struct. Eng. Mech.*, **60**(4), 567-594. http://doi.org/10.12989/sem.2016.60.4.567.

Shaheen, YBI, Soliman, NM, and Kandil, DE. (2013), "Influence of reinforced ferrocement concrete plates under impact load", *Int. J. Curr. Eng. Technol.*, **3**(4), 1528-1540.

Singh, G. (2005), "Finite element analysis of reinforced concrete shear walls", M.Sc. Thesis, Deemed University, India.

Subramani1, T. and Ramasamy, P. (2016), "Thermal conductivity of fibre filled with ferrocement sandwich panels", *Int. J. Appl. Innov. Eng. Manage.*, **5**(5), 204-215.

CC

Nomenclature

V_{rL}	= volume fraction in ferrocement element
N	=number of layers of mesh
n	=number of bars in one layer in the cross section
d_w	=diameter of mesh wire
t	=thickness of ferrocement layer for calculating the volume fraction in the layer
	=thickness of the web for calculating the volume fraction in the web
B	=width of the specimen
W_r	=unit weight of reinforcing mesh
γ_r	=density of reinforcing material
E_c	=modulus of elasticity of concrete
F_{cu}	=concrete characteristic compressive strength of concrete
ε	=concrete strain
ε_o	=concrete strain at compressive strength
P_{FC}	=1st crack load
P_{ser}	=serviceability load
P_{ult}	=ultimate load